Research Article | Vol. 26, No. 19 | 17 Sep 2018 | OPTICS EXPRESS 25492
Optics EXPRESS

# Efficiency improvement of up-conversion process of plasmonic-enhanced Er-doped-$NaYF_4$ nanoparticles under IR excitation

SARA ELRAFEI,[1,2,6] ISHAC KANDAS,[1,2,3,6,*] NADER SHEHATA,[1,2,3,4,6,] AND EFFAT SAMIR[2,5]

[1]*Department of Engineering Mathematics and Physics, Faculty of Engineering, Alexandria University, Alexandria 21544, Egypt*
[2]*Center of Smart Nanotechnology and Photonics (CSNP), Smart Critical Infrastructure (SmartCI) Research Center, Alexandria University, Alexandria 21544, Egypt*
[3]*Kuwait College of Science and Technology (KCST), Doha District, Safat 13133, Kuwait*
[4]*USTAR Bioinnovation Center, Faculty of Science, Utah State University, Logan, Utah 84341, USA*
[5]*Department of Electrical Engineering, Faculty of Engineering, Alexandria University, Alexandria 21544, Egypt*
[6]*These authors contributed equally to work*
[*]*ishac@vt.edu*

**Abstract:** The up-conversion process is extensively studied because of its wide variety of applications such as bioimaging, energy harvesting, and optical sensors. However, the optical conversion efficiency is still relatively low and needs to be improved. Therefore, this paper introduces a detailed study of improving the up-conversion emission efficiency through adding plasmonic metallic nanostructures to the up-conversion optical centers. Our idea is to couple the optical plasmonic resonance with the visible emission of the optical centers under IR excitation. The optical centers are erbium ions hosted by fluoride low-phonon environment. Our calculations consider most possible transitions that can occur between the optical centers; tri-valent erbium ions, through Judd-Ofelt analysis. In addition, the effect of changing some parametric values is discussed, such as irradiance, and multi-phonon relaxations, to show their optimum values which correspond to best quantum yield efficiency. By increasing the diameter of added gold nanoparticles (Au NPs), the probability of occupation has been increased, and consequently, both the luminescence and up-conversion efficiency have been increased.



## 1. Introduction

Optical up-conversion process has been studied over the last two decades to convert low-photon optical signal such as infra red (IR) to higher photon energies such as visible light. This conversion is applied in wide variety of applications such as optical sensors, energy harvesting, medical treatment, and bioimaging [1–14]. Rare earth tri-valent lanthanide ions are extensively used as optical up-conversion materials. Out of these optical lanthanides, erbium is one of the most efficient optical center for up-conversion process, due to its stable levels which can be excited by wide range of IR pumping wavelengths such as 780, 980, and 1550nm [15–18]. The erbium ions optical centers are recommended to be hosted by relatively low-phonon material for minimum optical losses during up-conversion process. One of the most famous hosts is sodium yttrium fluoride, $NaYF_4$, due to its relatively low phonon energy of the crystalline lattice compared to other hosts for erbium [19–21]. Regarding the analysis of optical up-conversion process, both experimental and analytical studies have been recently presented for erbium-doped-$NaYF_4$ under ~1520nm photon laser excitation via three-photon absorption based on Einstein coefficients in solar cell applications [22]. However, there is still a need of studying the same material under other excitation sources such as 780nm or 980nm via two-photon absorption mechanism, which is used in different sensing and medical

#341729 https://doi.org/10.1364/OE.26.025492
Journal © 2018 Received 7 Aug 2018; revised 6 Sep 2018; accepted 6 Sep 2018; published 14 Sep 2018

Optics EXPRESS

applications. Moreover, the role of plasmonic NPs in enhancing the up-conversion efficiency is still lacking within both detailed theoretical calculations and physical interpretation.

Moving in details to the transitions mechanisms of excited electrons in up-conversion process, the erbium electrons can occupy the excited states by two main mechanisms; ground state absorption (GSA) followed by excited state absorption (ESA) due to at least two-photon excitation, and energy transfer up-conversion (ETU). The last ETU process represents the interactions of electric dipole-dipole and the corresponding population of excited states [22–24]. ETU mechanism can be categorized in two sub-processes; energy transfer (ET) process from an excited ion to another one, while the second one is cross relaxation (CR) process related to the losses caused by the reversal of ET. In addition to the previously aforementioned main processes, there are other processes which influence both up-conversion transitions and corresponding efficiency such as multi-phonon relaxation (MPR) of nan-radiative excited electron relaxation, spontaneous emission (SPE) with no other depopulation transition, and stimulated emission (STE).

At variable excitation IR wavelengths, the up-conversion mechanisms are the same but the transitions differ. In this paper, we are focusing on 780nm excitation due to their different applications in sensors and biomedicine. Both laser photon excitations and the corresponding transitions are shown in Fig. 1 [24]. GSA process takes place after pumping $Er^{3+}$ ions by the first photon, and then the excited ion is transferred from $^4I_{15/2}$ (ground state) to populate $^4I_{9/2}$ level. Some electrons can make some relaxation to either $^4I_{11/2}$ or $^4I_{13/2}$ levels. Second photon can be responsible for ESA transition between $Er^{3+}$ ions to excited ions from $^4I_{11/2}$ level to populate either $^4F_{3/2}$ levelor $^2H_{11/2}$ by excited ions from $^4I_{13/2}$ level. ETU transition mechanism can have two possibilities; first one is from $^4I_{11/2}$ to $^4I_{15/2}$ level, as the acceptor ions gain excitation of electrons from $^4I_{11/2}$ to $^4F_{7/2}$.While for the other second ETU process, acceptor ions transfer from $^4I_{13/2}$ to occupy $^4F_{9/2}$ followed by a relaxation from $^4I_{11/2}$ to $^4I_{15/2}$ levels. All MPR processes are assumed to be non-radiative transitions. Our contribution in this paper is to introduce a theoretical study under near IR excitation wavelengths via two-photon absorption. Then, it will be shown the main parameters that affect emission quantum yield efficiencies with and without the added plasmonic nanostructure; gold nanoparticles (Au NPs).

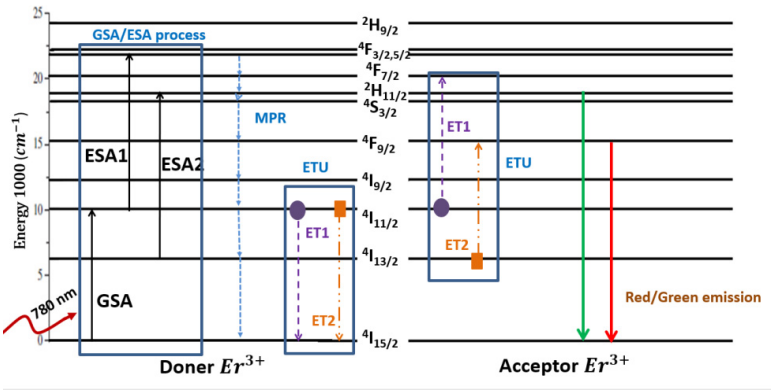


Fig. 1. Tri-valent erbium ions possible transitions under 780nm optical excitation.

## 2. Mathematical modeling

In this section, plasmonic mechanism has been analyzed in details to drive the enhancement in electric field due to the existence of plasmonic nanoparticles (NPs). Then, the up-conversion process is presented in mathematical model based on Einstein coefficients; $A_{if}$. Hence, the enhancement of up-conversion efficiency due to added plasmonic NPsis presented.

Optics EXPRESS

### 2.1 Plasmonic mechanism

Here it is introduced a complete study about the metal spherical surface and its impact on a single dipole emitter. The decay rates for emitting dipoles close to metal NPs are discussed. Furthermore, the localized field enhancement is presented in the vicinity of nano-metallic surface.

According to the exact electrodynamical theory, consider an atom as a single dipole with dipole moment $\mu$ is situated at distance $r$ from the center of a metallic NP that has radius $R$, and permittivity $\varepsilon_s = \varepsilon'_s + i\varepsilon''_s$ laid in a background medium of permittivity $\varepsilon_m$ [25]. Two different cases must be considered [26]. The first case (radial dipole orientation, PPOL); in which the direction of dipole moment is parallel to the surface of the NP. Meanwhile, in the other case (tangential dipole orientation, SPOL), the direction of the dipole is directed normal to the surface.

For easier calculations of the decay rates, the polarizability $\alpha(\omega)$ of the metallic nanoparticle should be expressed [27,28]:

$$\alpha(\omega) = \frac{\alpha_o(\omega)}{1 - i(k^3/6\pi)\alpha_o(\omega)} \tag{1}$$

where $\alpha_0(\omega)$ is the quasi-static polarizability. It is defined as the induced dipole moment per unit electric field. According to Clausius-Mossotti relation, $\alpha_0(\omega)$ is given by

$$\alpha_o(\omega) = 4\pi R^3 \frac{\varepsilon_s(\omega) - \varepsilon_m}{\varepsilon_s(\omega) + 2\varepsilon_m} \tag{2}$$

The expression of the normalized decay rates can be found. For PPOL ($\perp$), we have [27]

$$\gamma^{\perp}_{TOT} = 1 + \frac{3k^3}{2\pi}\mathrm{Im}[\alpha(\omega)\exp(2ikr)][\frac{-1}{(kr)^4} + \frac{2}{i(kr)^5} + \frac{1}{(kr)^6}] \tag{3}$$

$$\gamma^{\perp}_{rad} = 1 + \frac{3k^6}{4\pi}|\alpha(\omega)|^2[\frac{1}{(kr)^4} + \frac{1}{(kr)^6}] + \frac{k^3}{\pi}\mathrm{Re}(\alpha(\omega))\frac{1}{(kr)^3} \tag{4}$$

$$\gamma^{\perp}_{nonrad} = \frac{3k^3}{2\pi}\mathrm{Im}(\alpha(\omega)) - \frac{k^3}{6\pi}|\alpha(\omega)|^2[\frac{1}{(kr)^4} + \frac{1}{(kr)^6}] \tag{5}$$

On the other hand, for SPOL ($\parallel$), we have [27]:

$$\gamma^{\parallel}_{TOT} = 1 + \frac{3k^3}{8\pi}\mathrm{Im}(\alpha(\omega)\exp(2ikr)[\frac{1}{(kr)^2} + \frac{-2}{i(kr)^3} + \frac{-3}{(kr)^4} + \frac{2}{i(kr)^5} + \frac{1}{(kr)^6}] \tag{6}$$

$$\gamma^{\parallel}_{rad} = 1 + \frac{k^6}{16\pi}|\alpha(\omega)|^2[\frac{1}{(kr)^6} - \frac{1}{(kr)^4}] - \frac{k^3}{\pi}\mathrm{Re}(\alpha(\omega))\frac{1}{(kr)^3} \tag{7}$$

$$\gamma^{\parallel}_{nonrad} = \frac{3k^3}{8\pi}[\mathrm{Im}(\alpha(\omega)) - \frac{k^3}{6\pi}|\alpha(\omega)|^2][\frac{1}{(kr)^2} + \frac{-1}{(kr)^4} + \frac{1}{(kr)^6}] \tag{8}$$

where $\gamma_{rad}$, and $\gamma_{nonrad}$ are the normalized radiative and non-radiative decay rates, respectively, and the wave number $k = \sqrt{\varepsilon_m}\omega/c$ of emitted photon and c is the speed of light.Using metal nanospheres resonance, a high local filed intensity is produced. This high

Optics EXPRESS

field leads from the electric field confinement as a result of interaction of electrons and the incident field. According to the particle size and the surrounding media, we can control the resonance peak where a red shift is observed according to larger particle's radius. Such field can be used for enhancement the nonlinear nature of different processes. In normal photoluminescence, a linear relation with square of electric field enhancement $|E/Eo|^2$ is followed. On the contrary in UC, the field can be described by the relative enhancement factor $\gamma_E$ which is linear proportional to 2-N$^{th}$ power of electric field ratio because the UC is a two or a multi-photon process [29–31].By using certain excitation region, $\gamma_E$ can be expressed as [29,30]:

$$\gamma_E = \left|\frac{E}{E_o}\right|^{2N} \tag{9}$$

where*E*is the electric field at a certain position in the vicinity of metallic surface, $E_0$ is the electric field in the absence of the NPs and $N$ is the number of required photons for population. The angle-averaged local electric field enhancement factor is represented as [32]

$$\frac{E}{E_o} = 1 + \sum_{l=1}^{\infty} g_l^1(x_r)|b_l|^2 + g_l^2(x_r)|a_l|^2 \tag{10}$$

where $a_l, b_l$ are the Mie coefficients of the metal nanosphere that derived in details in [33].The Mie coefficients of the metal spheres are given as:

$$a_l = \frac{m\psi_j(\omega)\psi_j'(\upsilon) - \psi_j(\upsilon)\psi_j'(\omega)}{m\psi_j(\omega)\zeta_j'(\upsilon) - \psi_j(\omega)\zeta_j(\upsilon)} \tag{11}$$

$$b_l = \frac{\psi_j(\omega)\psi_j'(\upsilon) - m\psi_j(\upsilon)\psi_j'(\omega)}{\psi_j(\omega)\zeta_j'(\upsilon) - m\psi_j(\omega)\zeta_j(\upsilon)} \tag{12}$$

where $\psi_j$, $\zeta_j$ are Riccati_Bessel functions, $m = \sqrt{\varepsilon_s}/\sqrt{\varepsilon_m}$, $\upsilon = ka$ and $\omega = ma$. Moreover, bothfunctions $g_l^1(x_r)$) and $g_l^2(x_r)$ are given by [32]:

$$g_l^1(x_r) = \frac{2l+1}{2}\left|h_l^+(x_r)\right|^2 \tag{13}$$

$$g_n^2(x_r) = \frac{1}{2}((l+1)\left|h_{l-1}^+(x_r)\right|^2 + l\left|h_{l-1}^+(x_r)\right|^2) \tag{14}$$

where $x_r = kr$ and $h_l$ is the spherical Hankel function.There are different methods for modeling the dielectric constant of the metallic NPs, $\varepsilon_s$ [34]. In our model, Drude-critical pointsmodel is used as follows

$$\varepsilon_{DCP} = \varepsilon_\infty - \frac{\omega_p^2}{\omega^2 + i\gamma\omega} + \sum_{P=1}^{P=2} A_p\Omega_p\left[\frac{e^{i\phi_p}}{\Omega_p - \omega - i\Gamma_p} + \frac{e^{-i\phi_p}}{\Omega_p + \omega + i\Gamma_p}\right] \tag{15}$$

where $\varepsilon_\infty$ stands for the permittivity at $\omega=\infty$, $\omega_p$ is the plasma frequency $\gamma$ is damping coefficient, and P stands for the total number of the oscillators [35]. The typical values of used parameters would be shown later in Table 1.

Optics EXPRESS

### 2.2 Up-conversion modeling

The main parameter of UC mathematical model is Einstein coefficient, $A_{if}$, which is defined as the inverse of the radiative lifetime and correlated to calculations of transitions probabilities. The mathematical expression of $A_{if}$ is [22]:

$$A_{if} = \frac{64\pi^4 e^2}{3\hbar(2j+1)\lambda^3}\frac{n(n^2+2)^2}{9}S \tag{16}$$

where e is the electron charge, $\lambda$ is central wavelength according to a transition from initial state '*i*' to a final state '*f*', $\hbar$ is the reduced Planck's constant, *j* is the total angular momentum quantum number of the initial state, *n* is the refractive index(equals $\sqrt{\varepsilon_m}$)), and S is the electric dipole line strengths between all transitions, which is given by [22,36]:

$$S_{j\to j'} = \Omega_2[U^{(2)}]^2 + \Omega_4[U^{(4)}]^2 + \Omega_6[U^{(6)}]^2 \tag{17}$$

where $\Omega_i$ are the intensity parameters and $[U^{(i)}]^2$ are doubly reduced matrix elements related to the ionic transition from ground state, *j*to higher energy level, *j'*, undergoing the photon excitation. These parameters were calculated by Judd-Ofelt and found in a previous research as shown in ref [36]. In a related parameter, occupation rate of change $n_p^{\cdot}$ I s correlated to the relative occupation matrix $n_p$ through the matrices of different transition mechanisms as follows

$$n_p^{\cdot} = [M_{GSA} + M_{ESA} + M_{SPE} + M_{STE} + M_{MPR}]n_p + M_{ET} \tag{18}$$

where $M_{GSA}$, $M_{ESA}$, $M_{STE}$, $M_{SPE}$ and $M_{MPR}$ are matrices which describe GSA, ESA, STE, SPE, and MPR transitions, respectively. $M_{ET}$ is a matrix describing the ETU.A complete analysis of rate equation model including all matrices structure was discussed before in [37, 38].The transition probabilities of the discussed processes, except MPR, are presented as functions of the Einstein coefficients. Then, the UC luminescence, $Lum_{1f}$ from a higher level'*f*' to the ground level'1'is described by [37]:

$$L_{1f} = n_{p,f}A_{f1} \tag{19}$$

Regarding the UC efficiency, $\eta_{UC}$, for a certain transition, it can be calculated through the ratio between the emitted photons from excited levels by both SPE process and the stimulated absorbed photons, which can be mathematically described as follow [37]

$$\eta_{UC} = \frac{n_{oc.,i}A_{if}}{\sum n_{oc.,i}M_{GSA/ESA(f,i)} - \sum n_{p,f}M_{STE(i,f)}} \tag{20}$$

where $n_{oc.,i}$ is a relative occupation, $M_{GSA/ESA}$ is the transition probabilities of GSA and ESA, and $M_{STE}$ is the transition probabilities of STE. In case of 780 nm excitation, GSA/ESA probabilities are described together in the following matrix of Eq. (21), based on possible transitions from $^4I_{15/2}$ to $^4I_{9/2}$, from $^4I_{11/2}$ to$^4F_{3/2}$, and from $^4I_{13/2}$ to $^2H_{11/2}$.

Optics EXPRESS

$$M_{GSA\_ESA} = \frac{n\pi^2 c^2}{\hbar\omega_{12}^{\ 3}} . I_v . \begin{bmatrix} -\gamma_1 \frac{g_4}{g_1} A_{41} & 0 & 0 & 0 & 0 & 0 & 0 & 0 & 0 \\ 0 & -\gamma_2 \frac{g_7}{g_2} A_{72} & 0 & 0 & 0 & 0 & 0 & 0 & 0 \\ 0 & 0 & -\gamma_3 \frac{g_9}{g_3} A_{93} & 0 & 0 & 0 & 0 & 0 & 0 \\ \gamma_1 \frac{g_4}{g_1} A_{41} & 0 & 0 & 0 & 0 & 0 & 0 & 0 & 0 \\ 0 & 0 & 0 & 0 & 0 & 0 & 0 & 0 & 0 \\ 0 & 0 & 0 & 0 & 0 & 0 & 0 & 0 & 0 \\ 0 & \gamma_2 \frac{g_7}{g_2} A_{72} & 0 & 0 & 0 & 0 & 0 & 0 & 0 \\ 0 & 0 & 0 & 0 & 0 & 0 & 0 & 0 & 0 \\ 0 & 0 & \gamma_3 \frac{g_9}{g_3} A_{93} & 0 & 0 & 0 & 0 & 0 & 0 \end{bmatrix} \quad (21)$$

where $\gamma_1$ and $\gamma_2$ are damping factors representing the lower probability of the stimulated processes due to the energy mismatch between the transitions, while $g_i$ is the degeneracy of the energy level $i$ which has range from 1 to 9 according to the erbium metastable energy level [23]. STE matrix is the inverse process of GSA and ESA, which can be represented as follows in Eq. (22) under 780 nm excitation.

$$M_{STE} = \frac{n\pi^2 c^2}{\hbar\omega_{12}^{\ 3}} . I_v . \begin{bmatrix} 0 & 0 & 0 & \gamma_1 A_{41} & 0 & 0 & 0 & 0 & 0 \\ 0 & 0 & 0 & 0 & 0 & 0 & \gamma_2 A_{72} & 0 & 0 \\ 0 & 0 & 0 & 0 & 0 & 0 & 0 & 0 & \gamma_3 A_{93} \\ 0 & 0 & 0 & -\gamma_1 A_{41} & 0 & 0 & 0 & 0 & 0 \\ 0 & 0 & 0 & 0 & 0 & 0 & 0 & 0 & 0 \\ 0 & 0 & 0 & 0 & 0 & 0 & 0 & 0 & 0 \\ 0 & 0 & 0 & 0 & 0 & 0 & -\gamma_2 A_{72} & 0 & 0 \\ 0 & 0 & 0 & 0 & 0 & 0 & 0 & 0 & 0 \\ 0 & 0 & 0 & 0 & 0 & 0 & 0 & 0 & -\gamma_3 A_{93} \end{bmatrix} \quad (22)$$

### *3.3 Plasmonic effect on the up-conversion process*

In this section, the interaction between spherical metallic NPs with UC model is considered to improve the overall efficiency and luminescence. Considering an N-photon nonlinear UC process, the strength of UC local enhancement factor is proportional to 2-N$^{th}$ power of local optical field, so theoretically the local enhancement factor of electric field, $\gamma_E$ has been added to transition probabilities as shown in both Eqs. (23) and 24to modulate all stimulated process, *i.e* (GSA, ESA, and STE). The modified probability of GSA/ESA can be presented as [39,40]

$$W_{if,plasmon}^{GSA/ESA} = \gamma_E W^{GSA/ESA} = \frac{2n\pi^3 c^2}{h\omega_{ex}^2} I_v A_{if} \gamma_E \quad (23)$$

Optics EXPRESS

where $W^{GSA/ESA}$ is the GSA/ESA probability without added metal NPs. Meanwhile, the corresponding probability of STE can be expressed as follows [39,40]

$$W_{if,plasmon}^{STE} = \gamma_E W^{STE} = \frac{2n\pi^3 c^2}{h\omega_{ex}^2} I_v A_{if} \gamma_E . \quad (24)$$

Also, an enhancement factor for radiative transition $\gamma_{if,rad}$ can be represented due to the interaction between metallic plasmonic particles. This factor effects on the probability of SPE is for every transition from initial level, *i*, to final level, *f* [39,40]

$$W_{if}^{SPE} = \gamma_{if,rad} A_{if} . \quad (25)$$

On the contrary, there is another source of non-radiative losses, which has been grown up due to the transfer of energy from ($Er^{3+}$) ions to the metal NP. This factor is $\gamma_{if,nonrad}$ which would be also evaluated forthe required transitions from initial level, *i*, to final level, *f*. The probability of this loss can be represented as [39,40]

$$W_{if}^{loss} = \gamma_{if,nonrad} A_{if} . \quad (26)$$

Then, the ordinary differential equations are solved again, and the probabilities of occupation levels are determined assuming that the plasmonic NPs have negligible influence on energy transfer and multi-phonon relaxation processes. The new values of $n_p$ would be used to evaluate the green and the red emission luminescence and efficiencies.

Table 1 shows the values of the used parameters in up-conversion modeling based on other literature [41]. We used initial values for most of these parameters and then in the next sections, we will discuss the effect of varying these values on the efficiency. Refractive index; $n = 1.5$, was used as an average value between the possible values of *n* from 1.48 to 1.52 [40, 42].We are assuming that all parameters and analysis are carried out at room temperature as well as the analysis of the plasmonic NPs.

**Table 1. Parameters used in this model**

| Parameter | Value |
|---|---|
| Spectral frequency interval for illumination $\Delta w(s^{-1})$ [22] | $8.1\times10^{10}$ |
| $Er^{3+}$ ion concentration $N_0$ ($cm^{-3}$) [22] | $1.34\times10^{20}$ |
| Distance between $Er^{3+}$ ions $d_{Er\_Er}$(nm) [22] | 0.9 |
| Refractive index (n) [40] | 1.5 |
| Irradiance I ($W.m^{-2}$) | 1000 |
| Damping factors [22] | |
| $\gamma_1$ | 1.0 |
| $\gamma_2$ | 0.5 |
| $\gamma_3$ | 0.8 |
| Degeneracies value [43] | |
| $g_1$ | 8 |
| $g_2$ | 7 |
| $g_4$ | 5 |
| $g_7$ | 2 |
| $g_8$ | 2 |
| $g_9$ | 2 |
| MPR constants $W_{MPR}$ ($s^{-1}$) [22] | $10^8$ |
| k ($J^{-1}$) | $2.15\times10^{20}$ |
| Energy overlap integral [22] | |
| $K_{ET1}$ ($J^{-1}$) | $8\times10^{18}$ |
| $K_{ET2}$ ($J^{-1}$) | $1\times10^{18}$ |
| Distance between $Er^{3+}$ ion and gold $d_{Gold\_Er}$(nm) | 40 |

Optics EXPRESS

## 3. Results and discussions

### *3.1 Field enhancement and cross sections*

Here, the field enhancement of Au NPs close to $Er^{+3}$ions is shown with different radius to achieve the ultimate efficiency of UC process. In addition, the corresponding scattering cross section area is presented to explain the behavior of plasmon resonance as shown in Fig. 2.

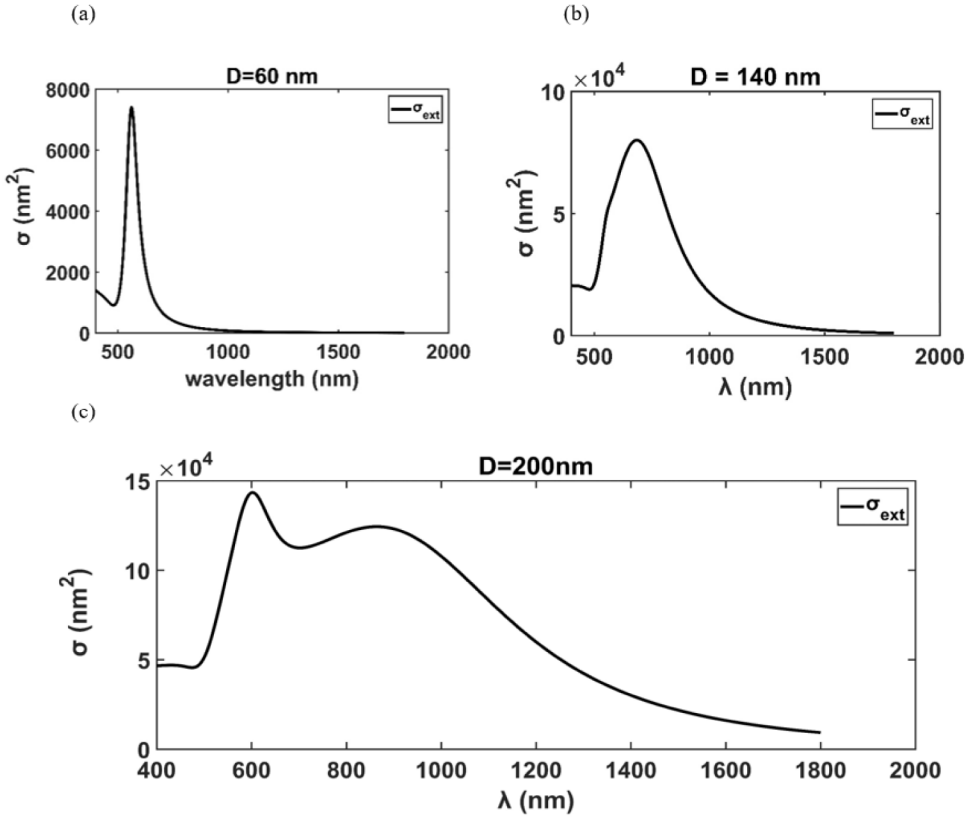


Fig. 2. The scattering cross sections area for Au particles with different diameters (a) D = 60nm,(b) D = 140nm, and (c) D = 200nm.

It is worthy to mention that for larger NPs, the resonance peaks are shifted for larger wavelength, which closer to the excitation wavelength. In our case the peak is shifted from 562nm to 866.7nm of D = 60nm, and 200nm, respectively.

Figure 3 shows the field enhancement factor, $\gamma_E$ averaged over the solid angle as a function of the wavelength. As seen in Fig. 3, the peak of $\gamma_E$ is also shifted to higher wavelength when the spherical radius is increased. At λ=780 *nm* which is the wavelength of the pump photon, $\gamma_E$ =101.4,373.7, and557.3 according to the used radius which are D = 60nm, 140 nm and 200 nm, respectively. The plasmonic effect is evident through the large values of this field that used to fulfill a considerable improvement in UC luminescence. This is because the UC process is always two or more photon absorption, which leads to a proportionality 2-$N^{th}$ power.

Optics EXPRESS

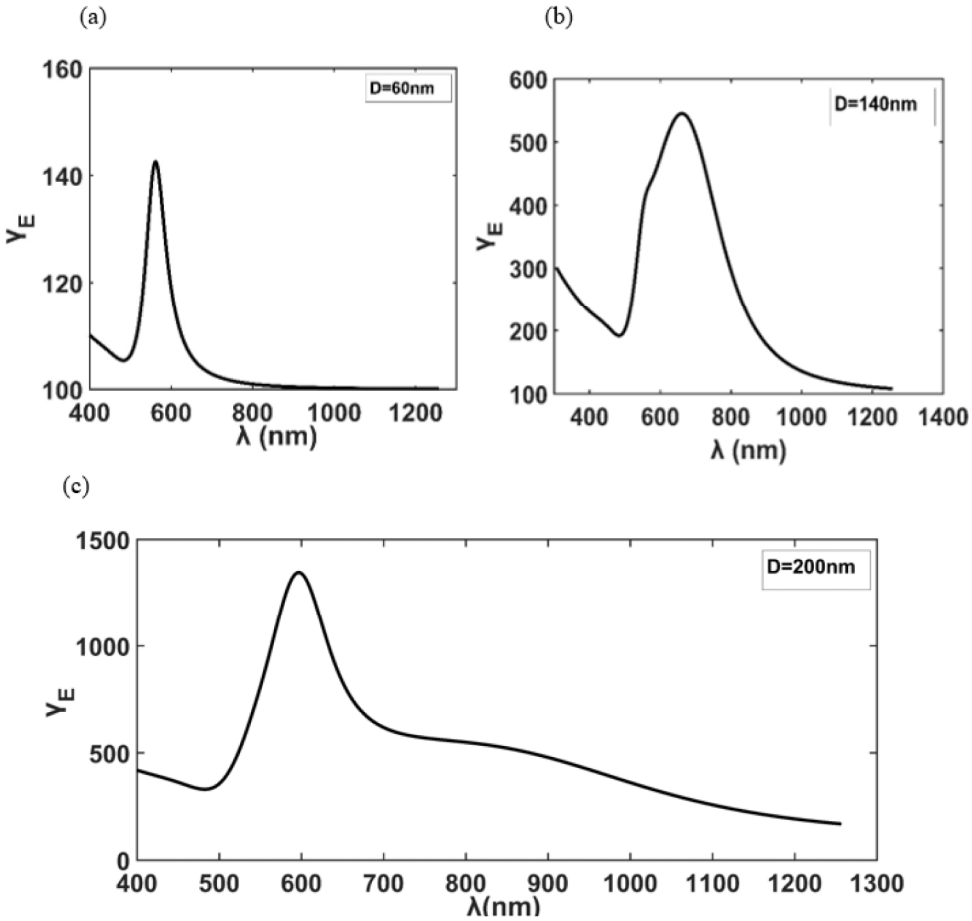


Fig. 3. Field enhancement ratio for Au particle (a) D = 60nm, (b) D = 140nm, and (c) D = 200nm.

Meanwhile, for every required transition from initial level, $i$ to final level, $f$, the normalized spontaneous radiative decay rate, $\gamma_{rad}$ and the non-radiative decay rates, $\gamma_{nonrad}$ decay rates are calculated. As a result of dipole orientation, $\gamma_{rad}$ and $\gamma_{nonrad}$ could be averaged over the different two orientations with different weight. For reducing the bad influence of the non-radiative losses, which lead to a heat production in Au NPs and slipping in the UC luminescence and efficiency, a proper distance should be guaranteed between Au NPs and trivalent ions [27].

### *3.2 Effect of Au NPs on UC luminescence and efficiency*

After employing the previous mentioned parameters with certain irradiance, the rate equation is solved again to calculate the occupation of every level. $^2H_{11/2}$, $^4S_{3/2}$and $^4F_{9/2}$levels' occupation is calculated and showed in Fig. 4. At the start of the operation without any source of excitation, the ground state is completely occupied and the others are empty.

Optics EXPRESS

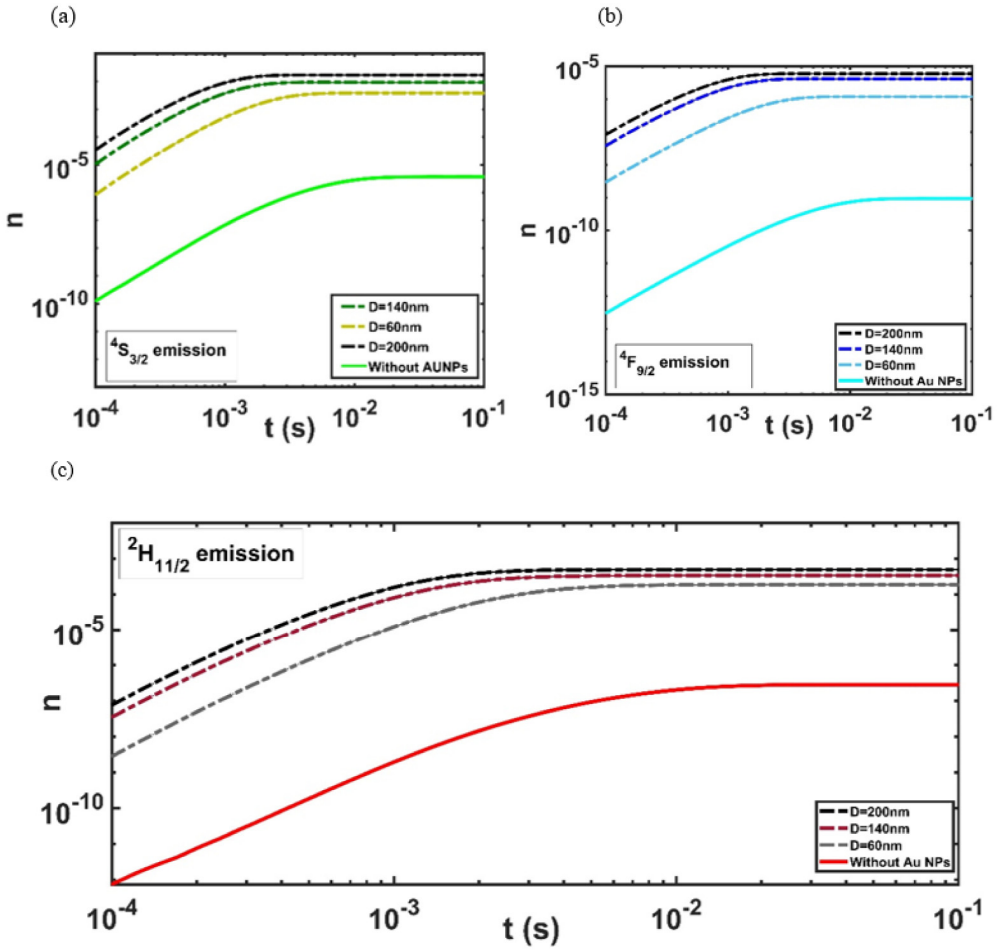


Fig. 4. The occupation change of different levels in both absence and presence of Au NPs with different radii close to Er ions as a function of time (a) $^4S_{3/2,}$ (b) $^4F_{9/2}$ and (c) $^2H_{11/2}$.

However, with 780 excitation, the higher level is gradually inclined before leveling off is occurred after approximately 40ms.It is clear that the electron population experienced a significant growth when applying the plasmonic resonance. Regarding the Diameter of 200 nm, $^2H_{11/2}$, $^4S_{3/2}$ and $^4F_{9/2}$ levels witnessed a dramatically enhancement, which is $7.5\times10^3$, $15\times10^3$, and $19.3\times10^3$, respectively. We notice that as the diameter increases, the enhancement factor becomes larger, and then the level populations increase, which rise both UC efficiency and luminescence.

Figure 5 shows various levels' luminescence emission versus time with adding Au NPs with different radii. As shown in Fig. 5, at saturation time 40ms the relative luminescence for $^2H_{11/2}$ is found to be $2.2\times10^3$, $5.1\times10^3$, and $9.1\times10^3$ for diameter 60 nm, 140 nm, and 200 nm, respectively. While for $^4S_{3/2}$, the luminescence increases with $3.1\times10^3$ fold for D = 60nm, $9.1\times10^3$ fold for D = 140nm, and $13.1\times10^3$ fold for D = 200 nm. In addition, the relative luminescence of $^4F_{9/2}$level is noticed to be $3.3\times10^3$, $12.7\times10^3$, and $22.7\times10^3$ for diameters 60nm, 140nm, and 200nm, respectively.

Optics EXPRESS

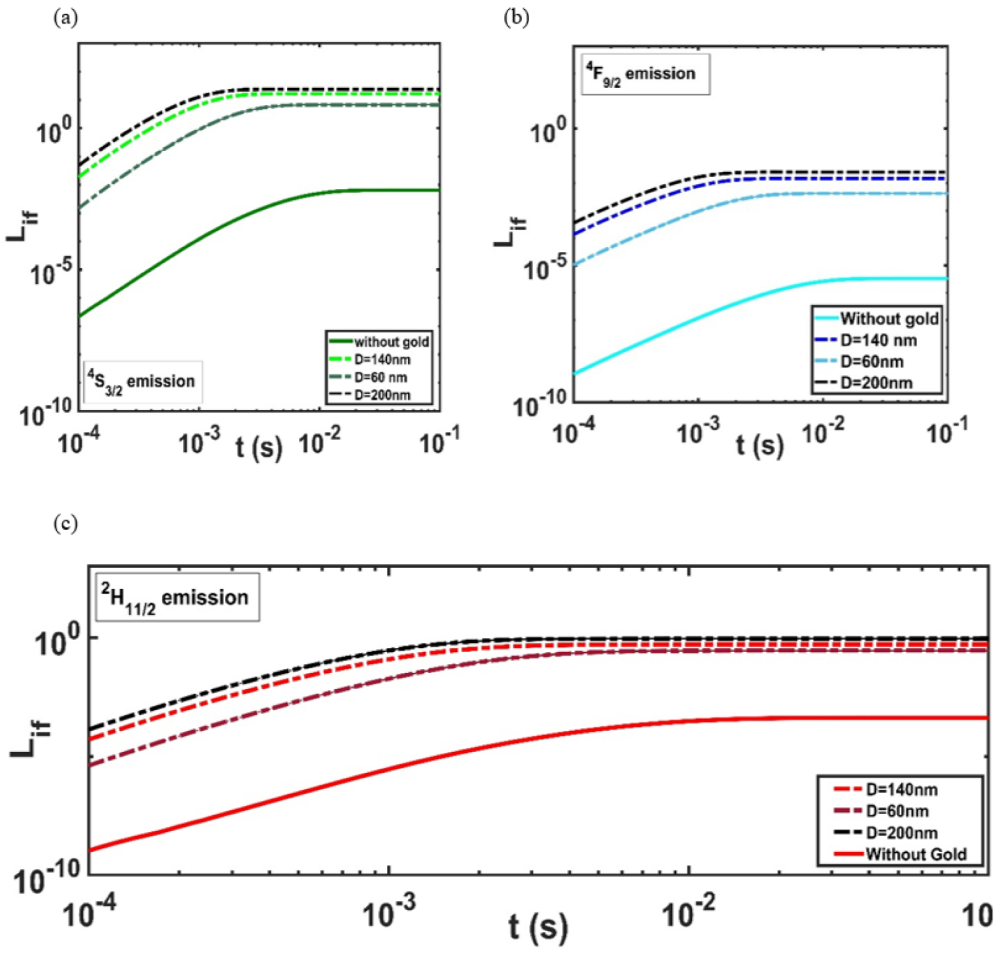


Fig. 5. The luminescence using different radii of Au NPs versus time of different levels (a) $^4S_{3/2}$, (b) $^4F_{9/2}$, and (c) $^2H_{11/2}$.

The UC efficiency depends on different parameters such as irradiance, which is presented in Fig. 6. Meanwhile, the impact of the Au NPs on UC efficiency is also clarified. As explained before, raising the irradiance intensity increases the red and green efficiency. Regarding the green emission, what stands out from the graph is that at the standard irradiance I = 1000 W/m$^2$the efficiency is enhanced from 0.73% to 8.9%, 11.2% and 13.4% that corresponding to 12.17-fold, 15.3-fold and 18.35-fold for diameter 60nm, 140nm, and 200nm, respectively. On the other hand, it is clearly to see that the efficiency is improved from 0.047 to 0.37 for D = 60 nm, 0.46 for D = 140nm and 0.632 for D = 200nm of red one.

As mentioned in mathematical model, for MPR process, $\Delta E_{if}$, $W_{MPR}$ and k are the main parameters that affect the transition probability [37]. Both $W_{MPR}$ and k are considered a material constant, which depend on host material's parameters. The $W_{MPR}$ represents the probability of sequential phonon transitions between different energy levels while k is required number of phonons for bonding the energy levels. Figure 7 shows the influence of MPR processes on UC efficiency. As shown in Fig. 7(a), at low k values, increasing k results in a decrease in the efficiencies because the $^2H_{11/2}$, $^4S_{3/2}$and $^4F_{9/2}$ depopulation decrease while, at high k values, growing k causes all the MPR transitions decreases. This leads to a decrease in the population of $^2H_{11/2}$, $^4S_{3/2}$ and $^4F_{9/2}$ from higher levels, which consequently experienced a decrease in the efficiencies. In contrast, In Fig. 7(b), it is obvious that the influence of $W_{MPR}$

Optics EXPRESS

is comparable but opposite to that of k. As expected, approximately, there are no effect on efficiencies in case of using Au NPs owing to the fact that the metal NPs have potential only on stimulated and spontaneous process.

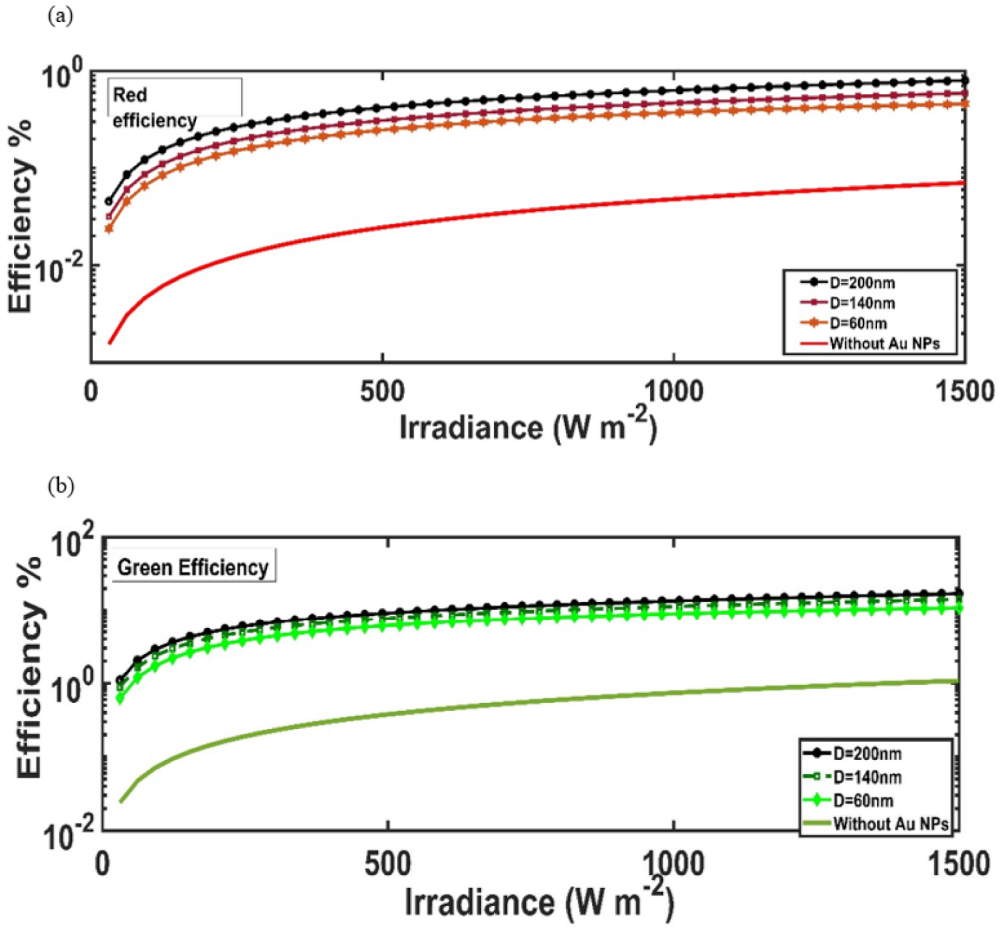


Fig. 6. UC efficiency verse irradiance in the absence and presence of Au NPs in proximity to Er ions for both emissions of (a) red, and (b) green.

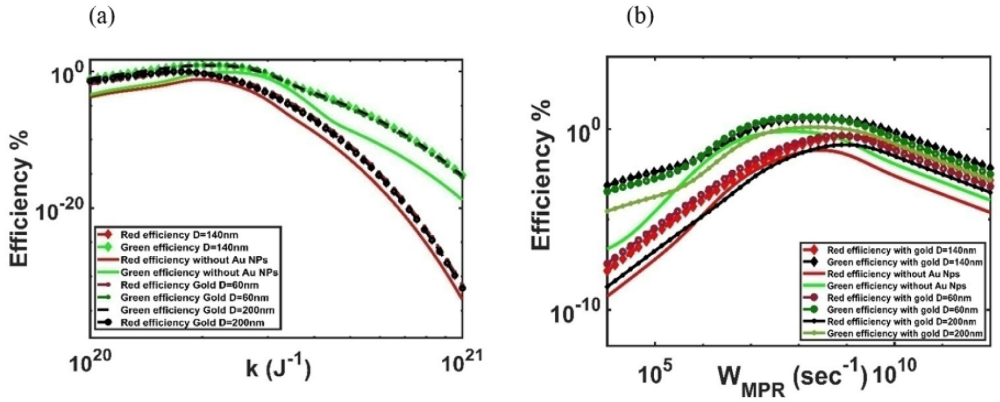


Fig. 7. The changing of green and the red efficiencies in the absence and presence of Au NPs with different radii according to the variation of (a) $K_{MPR}$, and (b) $W_{MPR}$.

Optics EXPRESS

On the other hand, the distance between Au NPs and $Er^{+3}$ ions has a great effect on the up-conversion efficiency. Figure 8 depicts the effect of changing the distance $d_{Gold\text{-}Er}$ on our system of Au NPs with diameter 60nm and $n$ = 1.5 of the surrounding medium .With regard to Fig. 8(a), it is clear that all decay rates either radiative or non-radiative witness a decline as distance increases. At the beginning, the non-radiative decay rate, $\gamma_{nonrad}$ is higher than the radiative decay rate $\gamma_{rad}$ until certain point at~27 nm, then the figure experiences an opposite behavior before leveling off. Consequently, it is obvious that the red and green efficiencies begin with small values then witness an increase before a gradual falling after ~at 25nm until reach almost saturation level as shown in Fig. 8(b).

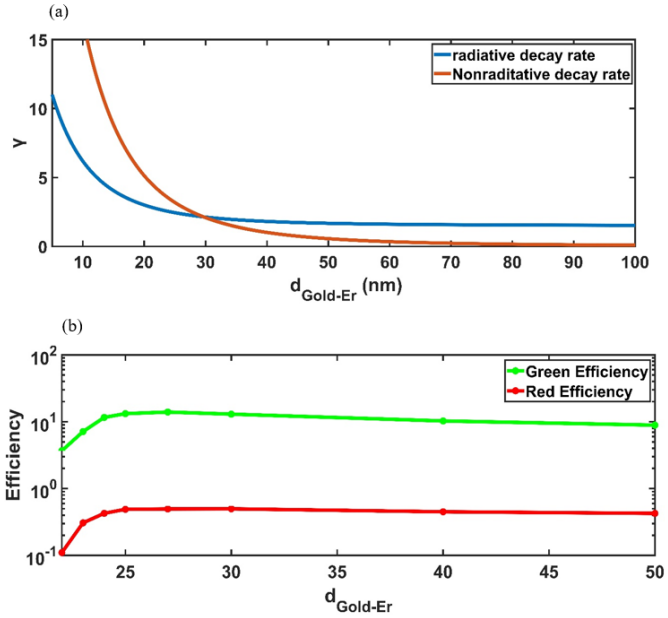


Fig. 8. The influence of changing the distance between Au NPs and Er ions $d_{Gold_Er}$on(a) Decay rates, and (b) Both green and red efficiencies for diameter D = 30nm and irradiance 1000 $W/m^2$.

## 4. Conclusion

This paper presents the impact of plasmonic NPs on improving the quantum efficiency of optical up-conversion (UC) process. Au NPs have been added to erbium-doped-$NaYF_4$NPs and then the whole material is analytically studied using Judd-Ofelt mechanism under near IR excitation. Firstly, general expressions of optical field enhancement, decay rates and their effects on transitions probability are studied due to the optical coupling between the plasmonic resonance and the emission of UC host. Then, the rate equation model that describes the UC is developed and correlated to the results for the spherical NPs. The simulations show the enhancement of occupation probability, luminescence, and up-conversion efficiency with added Au NPs. The increase of Au NPs diameters increase both plasmonic resonance wavelength and the bandwidth of plasmonic resonance spectrum, which lead to a better optical coupling with both up-conversion excitation and emission of erbium-doped fluoride host. This work can enhance the applications of UC nanomaterials in different medical, sensing and energy disciplines.

Optics EXPRESS

## References


1. A. Xia, Y. Deng, H. Shi, J. Hu, J. Zhang, S. Wu, Q. Chen, X. Huang, and J. Shen, "Polypeptide-Functionalized $NaYF_4$:$Yb^{3+}$,$Er^{3+}$ Nanoparticles: Red-Emission Biomarkers for High Quality Bioimaging Using a 915 nm Laser," ACS Appl. Mater. Interfaces **6**(20), 18329–18336 (2014).
2. C. F. Gainera, G.Joshuaa, and M. Romanowski," Toward the Use of Two-Color Emission Control in Upconverting NaYF4:$Er^{3+}$,$Yb^{3+}$ Nanoparticles for Biomedical Imaging," Nanoscale **8231**, 82310/1–8(2012).
3. F. C. van Veggel, C. Dong, N. J. Johnson, and J. Pichaandi, "$Ln^{3+}$-doped nanoparticles for upconversion and magnetic resonance imaging: some critical notes on recent progress and some aspects to be considered," Nanoscale **4**(23), 7309–7321 (2012).
4. B. Liu, C. Li, P. Ma, Y. Chen, Y. Zhang, Z. Hou, S. Huang, and J. Lin, "Multifunctional $NaYF_4$:Yb, Er@m$SiO_2$@$Fe_3O_4$-PEG nanoparticles for UCL/MR bioimaging and magnetically targeted drug delivery," Nanoscale **7**(5), 1839–1848 (2015).
5. J. H. Cho, M. Bass, S. Babu, J. M. Dowding, W. T. Self, and S. Seal, "Up-conversion luminescence of $Yb^{3+}$ – $Er^{3+}$ co doped $CeO_2$ nanocrystals with imaging applications," J. Lumin. **132**(3), 743–749 (2012).
6. N. Cockroft, "Application of energy upconversion spectroscopy to novel laser and phosphors design," J. Alloys Compd. **207-208**, 33–40 (1994).
7. R. Scheps, "Upconversion laser processes," Prog. Quantum Electron. **20**(4), 271–358 (1996).
8. D. Jaque, L. M. Maestro, E. Escudero, E. M. Rodrı'guez, J. A. Capobianco, F. Vetrone, A. J. delaFuente, F. Sanz-Rodrı'guez, M. C. Iglesias-de la Cruz, C. Jacinto, U. Rocha f, and J. G. Sole, " Fluorescent nano-particles for multi-photon thermal sensing," J. Lumin. **133**, 249–253 (2013).
9. F. Vetrone, R. Naccache, A. Zamarrón, A. Juarranz de la Fuente, F. Sanz-Rodríguez, L. Martinez Maestro, E. Martín Rodriguez, D. Jaque, J. García Solé, and J. A. Capobianco, "Temperature sensing using fluorescent nanothermometers," ACS Nano **4**(6), 3254–3258 (2010).
10. S. K. W. MacDougall, A. Ivaturi, J. Marques-Hueso, K. W. Krämer, and B. S. Richards, "Ultra-high photoluminescent quantum yield of β-$NaYF_4$: 10% $Er^{3+}$ via broadband excitation of upconversion for photovoltaic devices," Opt. Express **20**(S6), A879–A887 (2012).
11. A. Ivaturi, S. K. W. MacDougall, R. Martín-Rodríguez, M. Quintanilla, J. Marques-Hueso, K. W. Krämer, A. Meijerink, and B. S. Richards, "Optimizing infrared to near infrared upconversion quantum yield of β-$NaYF_4$:$Er^{3+}$ in fluoropolymer matrix for photovoltaic devices," J. Appl. Phys. **114**(1), 013505 (2013).
12. S. Fisher, J. C. Goldschmidt, K. W. Kramer, D. Biner, and M. Hermle, andS. W.Glunz,"calibrated photoluminescence measurements of the upconverter $NaYF_4$:20% $Er^{3+}$ for silicon solar cells," 25th European PV Solar Energy Conference and Exhibition, Valencia, Spain; 657–661(2010).
13. N. Shehata, M. Clavel, K. Meehan, E. Samir, S. Gaballah, and M. Salah, "Enhanced Erbium-Doped Ceria Nanostructure Coating to Improve Solar Cell Performance," Materials (Basel) **8**(11), 7663–7672 (2015).
14. C. Strumpela, M. McCanna, G. Beaucarneb, V. Arkhipovb, A. Slaouic, V. Svrcekc, C. del Canizod, and I. Tobiasd, "Modifying the solar spectrum to enhance silicon solar cell efficiency—An overview of available materials," Sol. Energy Mater. Sol. Cells **91**(4), 238–249 (2007).
15. I. Etchart, *Metal Oxides for Efficient Infrared to Visible Upconversion*, doctoral thesis chapter 3, pages 27- 42.
16. N. Shehata, K. Meehan, I. Hassounah, M. Hudait, N. Jain, M. Clavel, S. Elhelw, and N. Madi,"Reduced erbium-doped ceria nanoparticles: one nano-host applicable for simultaneous optical down- and up-conversions," Nanoscale Res Lett. **9**(1), 231 (2014).
17. R. B. Anderson, S. J. Smith, P. S. May, and M. T. Berry, "Revisiting the NIR-to-Visible Upconversion Mechanism in β-NaYF4:$Yb^{3+}$,$Er^{3+}$," J. Phys. Chem. Lett. **5**(1), 36–42 (2014).
18. S. Tanabe, S. Yoshii, K. Hirao, and N. Soga, "Upconversion properties, multiphonon relaxation, and local environment of rare-earth ions in fluorophosphate glasses," Phys. Rev. B Condens. Matter **45**(9), 4620–4625 (1992).
19. D. N. Patela, A. Lewis, D. M. Wright, D. Lewisa, R. Valentinea, M. Valentinea, D. Wessleya, S. Sarkisovb, andA. M. Darwishc, "Optical properties and size distribution of the nano-colloids made of rare-earth ion-doped nayf4;SPIE 9359: 93591L(1-9).
20. Z. Li, W. Park, G. Zorzetto, J.-S. Lemaire, and C. J. Summers, "Synthesis Protocols for δ-Doped $NaYF_4$:Yb,Er," Chem. Mater. **26**(5), 1770–1778 (2014).
21. J. Chen and J. X. Zhao, "Upconversion nanomaterials: synthesis, mechanism, and applications in sensing," Sensors (Basel) **12**(3), 2414–2435 (2012).
22. S. Fischer, H. Steinkemper, P. Löper, M. Hermle, and J. C. Goldschmidt, "Modeling upconversion of erbium doped microcrystals based on experimentally determined Einstein coefficients," J. Appl. Phys. **111**(1), 013109 (2012).
23. H. Guo, "Green and red upconversion luminescence in $CeO_2$:$Er^{3+}$ powders produced by 785nm laser," J. Solid State Chem. **180**(1), 127–131 (2007).
24. M. Simeckova, D. Jacquemarta, L. S. Rothmana, R. R. Gamacheb, and A. Goldmanc, "Einstein A-coefficients and statistical weights for molecular absorption transitions in the HITRAN database," J. Quant. Spectrosc. Radiat. Transf. **98**(1), 130–155 (2006).
25. G. Colas des Francs, A. Bouhelier, E. Finot, J. C. Weeber, A. Dereux, C. Girard, and E. Dujardin, "Fluorescence relaxation in the near-field of a mesoscopic metallic particle: distance dependence and role of plasmon modes," Opt. Express **16**(22), 17654–17666 (2008).

Optics EXPRESS


26. F. Hallermann, C. Rockstuhl, S. Fahr, G. Seifert, S. Wackerow, H. Graener, G. V. Plessen, and F. Lederer, "On the use of localized plasmon polaritons in solar cells," Phys. Status Solidi (a) **205**(12), 2844–2861 (2008).
27. R. Carminati, J. J. Greffet, C. Henkel, and J. M. Vigoureux, "Radiative and non-radiative decay of a single molecule close to a metallic nanoparticle," Opt. Commun. **261**(2), 368–375 (2006).
28. B. T. Draine, "The discrete-dipole approximation and its application to interstellar graphite grains," Astrophys. J. **333**, 848–872 (1988).
29. X. Chen, W. Xu, L. Zhang, X. Bai, S. Cui, D. Zhou, Z. Yin, H. Song, and D. H. Kim, "Large Upconversion Enhancement in the "Islands" Au–Ag Alloy/NaYF4: $Yb^{3+}$, $Tm^{3+}$/$Er_3^+$ Composite Films, and Fingerprint Identification," Adv. Funct. Mater. **25**(34), 5462–5471 (2015).
30. W. Xu, X. Chen, and H. Song, "Upconversion manipulation by local electromagnetic field," Nano Today **17**, 54–78 (2017).
31. X. Liu and D. Y. Lei, "Simultaneous excitation and emission enhancements in upconversion luminescence using plasmonic double-resonant gold nanorods," Sci. Rep. **5**(1), 152351 (2015).
32. R. Colom, A. Devilez, N. Bonod, and B. Stout, "Optimal interactions of light with magnetic and electric resonant particles," Phys. Rev. B **93**(4), 045427 (2016).
33. F. B. Craig, F. Bohren, and D. R. Huffman, *Absorption and scattering of light by small particles*, Inc: John Wiley & Sons, New York, USA, 1983.
34. F. Hao and P. Nordlander, "Efficient dielectric function for FDTD simulation of the optical properties of silver and gold nanoparticles," Chem. Phys. Lett. **446**(1–3), 115–118 (2007).
35. A. Vial and T. Laroche, "Comparison of gold and silver dispersion laws suitable for FDTD simulations," Appl. Phys. B **93**(1), 139–143 (2008).
36. J. Yang, M. Diemeer, L. T. Hilderink, R. Dekker, and A. Driessen, "Judd-Ofelt analysis of Nd (TTa) 3Phen-doped 6-FDA/Epoxy planar waveguides," In11th Annual Symposium IEEE/LEOS Benelux 2006 Nov 30. IEEE/LEOS Benelux Chapter.
37. E. Samir, N. Shehata, M. Aldacher, and I. Kandas, "Parametric study of up-conversion efficiency in Er-doped lanthanide hosts under 780 nm/980 nm excitation wavelengths," J. Electron. Mater. **45**(6), 2732–2744 (2016).
38. C. Z. Hadad and S. O. Va'squez, "Energy-transfer processes induced by exchange interactions," Phys. Rev. B **60**(12), 8586–8594 (1999).
39. S. Fischer, F. Hallermann, T. Eichelkraut, G. von Plessen, K. W. Krämer, D. Biner, H. Steinkemper, M. Hermle, and J. C. Goldschmidt, "Plasmon enhanced upconversion luminescence near gold nanoparticles--simulation and analysis of the interactions: Errata," Opt. Express **21**(9), 10606–10611 (2013).
40. B. Herter, S. Wolf, S. Fischer, J. Gutmann, B. Bläsi, and J. C. Goldschmidt, "Increased upconversion quantum yield in photonic structures due to local field enhancement and modification of the local density of states--a simulation-based analysis," Opt. Express **21**(S5 Suppl 5), A883–A900 (2013).
41. H. Guo, "Green and red upconversion luminescence in CeO2: $Er^{3+}$ powders produced by 785 nm laser," J. Solid State Chem. **180**(1), 127–131 (2007).
42. A. Ivaturi, S. K. MacDougall, R. Martín-Rodríguez, M. Quintanilla, J. Marques-Hueso, K. W. Krämer, A. Meijerink, and B. S. Richards, "Optimizing infrared to near infrared upconversion quantum yield of β-$NaYF_4$: $Er^{3+}$ in fluoropolymer matrix for photovoltaic devices," J. Appl. Phys. **114**(1), 013505 (2013).
43. K. Wynne and R. M. Hochstrasser, "Coherence effects in the anisotropy of optical experiments," Chem. Phys. **171**(1–2), 179–188 (1993).